STEREO/SECCHI/COR1 Calibration and Measurement Algorithms Document (CMAD)

Revision	Effective Date	Description of Changes
Baseline	06/30/2021	First release
Revision 1	12/06/2021	Updated references
Revision 2	03/09/2025	Added section on tomographic reconstruction
Revision 3	04/15/2026	Minor corrections

1. Introduction

The COR1 telescope is the inner coronagraph of the Sun Earth Connection Coronal and Heliospheric Investigation (SECCHI) instrument suite aboard the twin Solar Terrestrial Relations Observatory (STEREO) spacecraft. Like all coronagraphs, COR1 is designed to measure the weak light from the solar corona in the presence of scattered light from the much brighter solar photosphere. It is a classic Lyot internally occulting refractive coronagraph (Lyot, 1939) which is designed to observe the white light corona from 1.4 to 4 $R_{\odot}$. This covers the coronal region between the SECCHI Extreme Ultraviolet Imager (EUVI) and the outer coronagraph COR2, thus providing an uninterrupted view of the corona from the solar surface to the outer edge of the COR2 field-of-view, or out to as far as 1 AU for features that appear in the SECCHI Heliospheric Imager (HI) fields-of-view. The COR1 design is the first space-borne internally occulted *refractive* coronagraph, in contrast to the LASCO/C1 (Brueckner *et al*., 1995) which was an internally occulted *reflective* design. A complete description of the COR1 telescope is given in Howard *et al*. (2008). The design of the COR1-A and COR1-B telescopes on STEREO-A and STEREO-B are identical except for slightly different occulter sizes reflecting the different perihelion distances of each spacecraft.

The goal of COR1 is to study the properties of coronal mass ejections (CMEs) via observations of the brightness of Thomson-scattered light from the solar K-corona in both total brightness *B* and linearly polarized brightness *pB*. These measurements, combined with those from the other SECCHI telescopes, aim to answer the questions:

- What is the timing of physical properties involved in CME initiation? What are the structures involved in CME initiation?
- What is the 3-dimensional structure and kinematic properties of CMEs?
- What is the 3-dimensional structure of active regions, coronal loops, helmet streamers, etc.?
- What are the critical forces controlling the properties of CMEs in the corona and interplanetary medium?

Measuring the K-corona polarization properties offers several advantages. One is that measuring polarized brightness *pB* assists in separating out the fainter but highly polarized K-corona signal from the brighter but largely unpolarized instrumental scattered light. This is especially useful for studying stable features such as helmet streamers through tomographic techniques. Experience in flight has also shown good success in separating out the time-varying total brightness signal *B* in CMEs from the more static combination of the background K-corona and instrumental stray light. In that case, the ratio *pB*/*B* contains useful information about the scattering geometry, from which can be derived information about the 3-dimensional structure of the CME.

Figure 1 shows the COR1 optical layout. A feature of the COR1 design is that a Corning Polarcor linear polarizer is in the optical path at all times. This polarizer can be rotated around its optical axis to sample the linear polarization properties of the coronal radiation. The normal operating mode of COR1 is to take three images in rapid succession, at linear polarization angles of 0°, 120°, and 240°. From these three images can be calculated the total brightness B, polarized brightness pB, and angle of polarization μ, using the procedure outlined in Billings (1966). When necessary to reduce telemetry volume, images at the same three polarization angles are summed onboard the spacecraft into a single image, from which only the total brightness can be derived. Operating the detector in exactly the same way for both the normal three-image polarization mode and single-combined-image reduced telemetry mode ensures that there are no calibration issues in comparing the total brightness from both modes. These combined images are alternated with the normal three polarized image sequences so that total brightness is observed at the normal cadence, while polarized brightness and angle are observed at reduced cadence. The need to combine COR1 images on-board to reduce telemetry is fairly rare—the vast majority of the time the COR1 polarization data come down at full cadence.

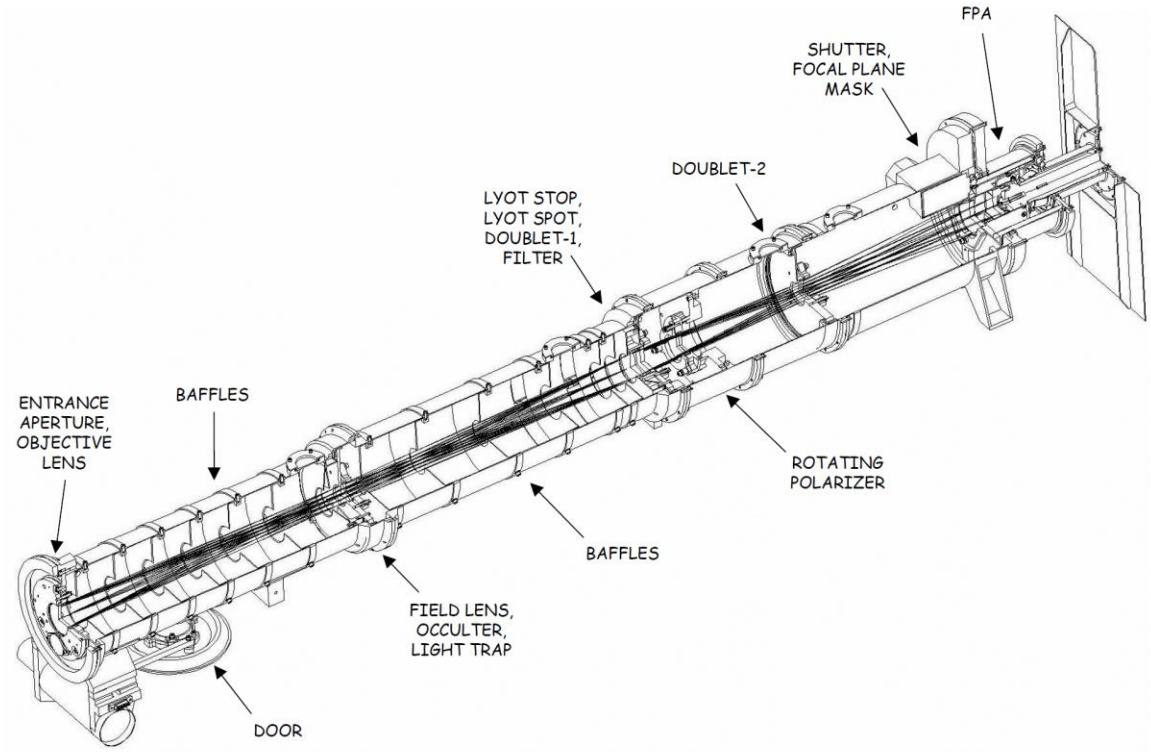

Figure 1. COR1 optical layout.

Although the COR1 detector has 2048×2048 pixels, with each pixel representing a 3.75×3.75 arcsecond region of the sky, the normal mode of operation is to sum the pixels onboard into larger binned pixels. One reason for doing this is to reduce the amount of telemetry, but this also increases the signal-to-noise in the resulting binned pixels. In addition, the error budget for the optical point spread function was more consistent with 2×2 binned pixels than with the full detector resolution. From launch until 19 April 2009 the normal COR1 mode of operations was to bin images to 1024×1024 (7.5”×7.5”), after which the images were binned to 512×512 (15”×15”) on both spacecraft to reflect the lower telemetry rate with increasing solar distance. Given the aging of the thermal blankets leading to increased temperatures of the optical bench, the intent is to continue to bin to 512×512 even as the available telemetry rate increases as the STEREO spacecraft reapproach Earth.

The various algorithms described in this document are listed below

Section 2	Conversion from Level 0 to Level 1
Section 3	Derivation of polarization parameters
Section 4	Background determination
Section 5	Electron density tomographic inversion

1.1 Purpose

This document describes the process used to convert from raw COR1 Level 0 images to calibrated Level 1 images, and the subsequent derivation of the total brightness *B*, the polarized brightness *pB*, and the angle of polarization μ. The Level 0 data are stored in FITS format, as described in [**PIPELINE**]. All calibration files are distributed as part of the SECCHI software package in SolarSoft.

1.2 Contents

Section 2 describes the procedure used to convert COR1 images from raw Level 0 to calibrated Level 1, which is the basic step needed for all subsequent scientific analysis. Section 3 describes how to use these calibrated images to derive the linear polarization properties of the coronal radiation. Section 4 describes the procedure used for estimating the instrumental and F-corona background. Section 5 describes the tomography method for reconstructing 3D electron density of the corona using *pB* images observed from STEREO/COR1.

1.3 References

[PIPELINE] STEREO/SECCHI Level-0 to Level-0.5 FITS Pipeline CMAD, STEREO_SECCHI_Reduce_CMAD_20211206.pdf, Version 1.1, 06 December 2021

Billings, D. E., 1966, A Guide to the Solar Corona, New York: Academic Press.

Brueckner, G. E., Howard, R. A., Koomen, M. J., Korendyke, C. M., Michels, D. J.; Moses, J. D., Socker, D. G., Dere, K. P., Lamy, P. L., Llebaria, A., Bout, M. V.; Schwenn, R., Simnett, G. M., Bedford, D. K., Eyles, C. J., 1995, The Large Angle Spectroscopic Coronagraph (LASCO), *Solar Phys*., **162**, 357–402.

Howard, R. A., Moses, J. D., Vourlidas, A., Newmark, J. S., Socker, D. G., Plunkett, S. P.; Korendyke, C. M., Cook, J. W., Hurley, A., Davila, J. M., Thompson, W. T., St Cyr, O. C.; Mentzell, E., Mehalick, K., Lemen, J. R., Wuelser, J. P., Duncan, D. W., Tarbell, T. D.; Wolfson, C. J., Moore, A. Harrison, R. A., Waltham, N. R., Lang, J., Davis, C. J.; Eyles, C. J., Mapson-Menard, H., Simnett, G. M., Halain, J. P., Defise, J. M., Mazy, E.; Rochus, P., Mercier, R., Ravet, M. F., Delmotte, F., Auchere, F., Delaboudiniere, J. P.; Bothmer, V., Deutsch, W., Wang, D., Rich, N., Cooper, S., Stephens, V., Maahs, G.; Baugh, R., McMullin, D., Carter, T., 2008, Sun Earth Connection Coronal and Heliospheric Investigation (SECCHI), *Space Sci. Rev.*, **136**, 67–115.

Lyot, B., 1939, The study of the solar corona and prominences without eclipses (George Darwin Lecture, 1939), *Mon. Not. Royal Astron. Soc*., **99**, 580–594.

2. Conversion from Level 0 to Level 1

2.1 Overview

Conversion of SECCHI telemetry into Level 0 FITS files is described in **[PIPELINE]**. Here we describe the process of converting from raw Level 0 data to calibrated Level 1 data. This procedure is applied through the IDL routine `secchi_prep.pro` in the SolarSoft library. **[SECCHI_PREP]** gives an overview

of the SECCHI_PREP routine. Here we describe the specific steps that are applied to COR1 data, which are implemented through the IDL routine `cor1_calibrate.pro` in SolarSoft, which is called from SECCHI_PREP.

2.1.1 Heritage

This procedure is developed from that used for the SECCHI/COR2 telescope, and is essentially the same for all white-light solar coronagraphs.

2.1.2 Product Description

The process of applying calibration to COR1 Level 0 data to produce Level 1 data consists of converting raw detector signals in data numbers (DN) into Mean Solar Brightness (MSB) units. MSB is defined as the average surface brightness of the solar disk, if the instrument (i.e. COR1) were to observe the Sun directly. Unless otherwise specified, the output image is the same size and format as the input image, with each input and output pixel in a one-to-one correspondence with each other.

2.2 Theoretical Description

The basic process of converting from raw DN to calibrated MSB can be described as follows:

$$MSB = \left(\frac{c}{V}\right)\left(\frac{DN - DN_0}{\delta t} - B\right)$$

where DN_0 is the detector bias, δt is the exposure time, B is an estimate of the instrumental background, V is the instrumental vignetting function, and c is the calibration factor. The parameters DN_0 and δt are determined onboard and come down in the telemetry. Options exist within SECCHI_PREP to omit any or all of the steps in the calibration process.

2.3 Error Analysis and Corrections

Raw COR1 images are dominated by scattered light. This is demonstrated in Figure 1, which shows a horizontal trace through the center of a COR1-A image from early in the mission. The black line shows raw data, with only the bias DN_0 removed; the red line includes background subtraction. Generally speaking, the signal is only a few percent of the raw data. Figure 3 shows the predicted signal-to-noise ratio based on pre-flight data for COR1-A as a function of various exposure times.

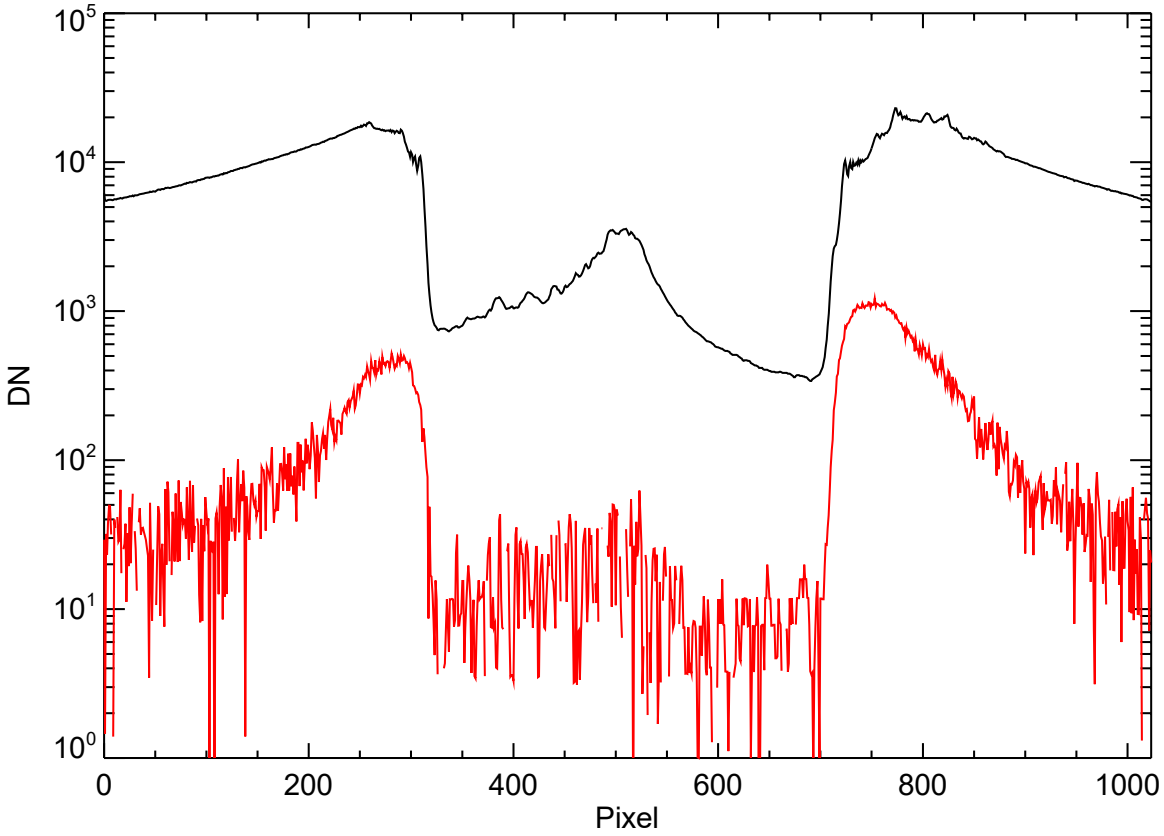

Figure 2. Comparison of signal (red) to raw uncorrected data (black), for a horizontal trace through the center of a COR1-A image early in the mission.

As the mission has progressed, the amount of instrumental scattering has increased due to new dust particles attaching themselves to the front objective. COR1-A has also shown asymmetrical evolution in the background due to motions of the occulter stem caused by thermal evolution. These changes have driven changes in the COR1-A exposure times. The following table gives the history of exposure times used with COR1-A.

Date	Exposure Time (sec)
After commissioning	1.7
12 August 2011	1.5
16 March 2012	1.0
15 March 2016	0.7

Although COR1-B also saw changes in the instrumental background with time, the COR1-B exposure time remained at 1.7 seconds up to the loss of contact with the STEREO-B spacecraft in October 2014.

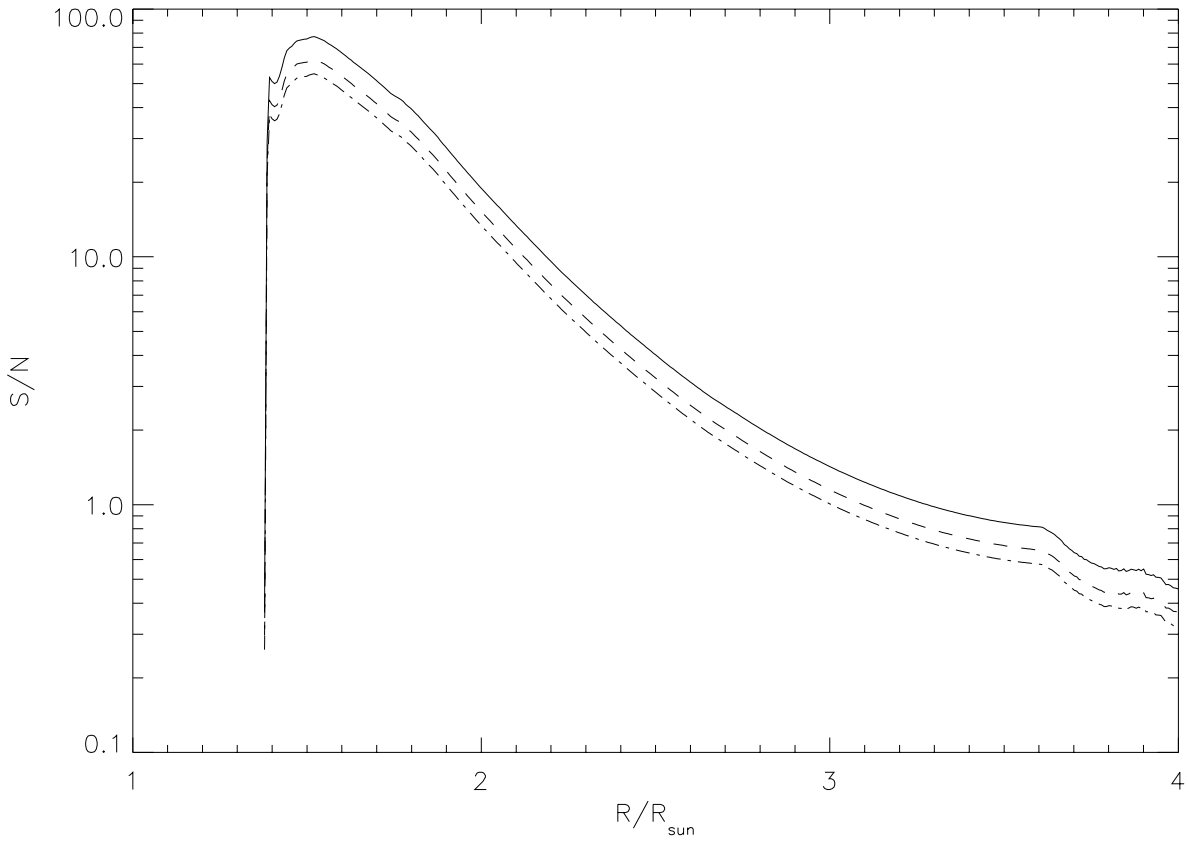

Figure 3. Average signal-to-noise ratio for COR1-A as a function of radial distance for exposure times of 2 seconds (solid), 1.3 seconds (dashed), and 1 second (dash-dot).

2.4 Calibration and Validation

2.4.1 Calibration

2.4.1.1 Pre-flight/On-ground Calibration

Pre-flight measurements of the COR1 telescope were designed to verify the performance prior to delivery for integration into the SECCHI instrument suite. These tests proceeded in two phases, first

with a Meade telescope in the COR1 assembly facility in Building 5 at NASA Goddard Space Flight Center, followed by more extensive testing in a vacuum tunnel facility at the Naval Research Laboratory designed specifically for testing solar coronagraphs.

Stimulus	Quantity	Data Products Affected
Meade telescope	• Focus • Polarization angle • Polarizer image motion • Exposure time accuracy and repeatability • Light leaks • Boresight	• Level 1 and derived products
NRL A13 coronagraph vacuum tunnel facility	• Flat field / vignetting • Plate scale • Scattered light • Resolution • Photon curve • Radiometric calibration • Polarization response • Signal-to-noise ratio	• Level 1 and derived products

For the purposes of calibrating observations taken during flight, the pre-flight measurements are superseded by in-flight calibration activities with one exception: It was determined during testing that the alignment of the linear polarizer on COR1-A differed by 11.04 ± 0.28 degrees from the zero position on the hollow core motor, corresponding to 4.4 ± 0.1 motor steps. For this reason, observations with COR1-A are made with a 4-step offset to the polarizer position. For COR1-B, this same angle was found to be 0.79 ± 1.01 degrees (0.32 ± 0.40 steps), consistent with zero. Thus, no offset is applied to COR1-B observations.

2.4.1.2 In-flight Calibration

Extensive work has been done on calibrating the in-flight performance of the COR1 telescopes. Thompson and Reginald (2008) used observations of the planet Jupiter, between 29 November to 2 December 2007 from COR1-A, and between 15–18 January 2008 from COR1-B, to derive the absolute radiometric calibration of COR1 on each STEREO spacecraft. Although very bright, the disk of the planet covered several pixels on the detector, and therefore stayed below saturation. The integrated brightness of Jupiter in MSB units depends on the distance of Jupiter from both the Sun and the spacecraft at the time of observation, and on the planetary albedo, which was taken from Chanover *et al*. (1996). The resulting calibration factors c (MSB s/DN) of 6.578×10^{-11} for COR1-A, and 7.080×10^{-11} for COR1-B, agreed well with the rougher pre-flight measurements. The major source of uncertainty is the uncertainty in the planetary albedo of Jupiter of 5–10%.

Thompson and Reginald (2008) also determined the pointing calibration of the two telescopes. From 24–26 February 2007, COR1-B observed the Moon pass in front of the solar corona. This provided a unique opportunity to establish the absolute pointing. Circles were fitted to the extremely sharp edges

of the Moon's disk as it moved across the field. This allowed the center position of the Moon to be established to subpixel accuracy. These pixel positions were then compared against highly precise ephemeris calculations, taking both light travel time and stellar aberration into account. From these measurements were determined the sun center position, the plate scale, and the roll offset of COR1-B relative to the spacecraft. A similar analysis was performed for COR1-A using the bright star λ Aquarii, which passed through the field-of-view from 28 February–2 March 2007.

Thompson, W.T. (2018) uses observations of several bright stars which periodically pass through the COR1 fields of view to track changes in the radiometric calibration over time. It was found that by 1 October 2014, when contact was lost with the STEREO-B spacecraft, the loss in sensitivity in COR1-B was 1.7%, while COR1-A was down by 4.4%. As of 1 November 2017, the COR1-A decline was estimated to be 6.4%. These rates of decline are incorporated into the SECCHI processing routines. The same star observations are also used to track any changes in the telescope pointing, but so far no changes have been detected. Monitoring of star brightnesses and positions is ongoing.

Embedded in the door of each COR1 telescope is a diffuser window. This diffuser window is sized so that when the door is closed and the diffuser is illuminated by the Sun, the full COR1 field-of-view is illuminated without vignetting. Thus, images of this door can be used to derive the COR1 vignetting function. An example image is shown in Figure 4. This image has been colorized and processed to bring out some of the faint features. Most of the field is unvignetted, and shows up as white in Figure 4. The central portion is blocked by the combination of the occulter and the focal plane mask, and the corners are blocked by the field stop. Vignetting occurs at the edges of the occulted sections.

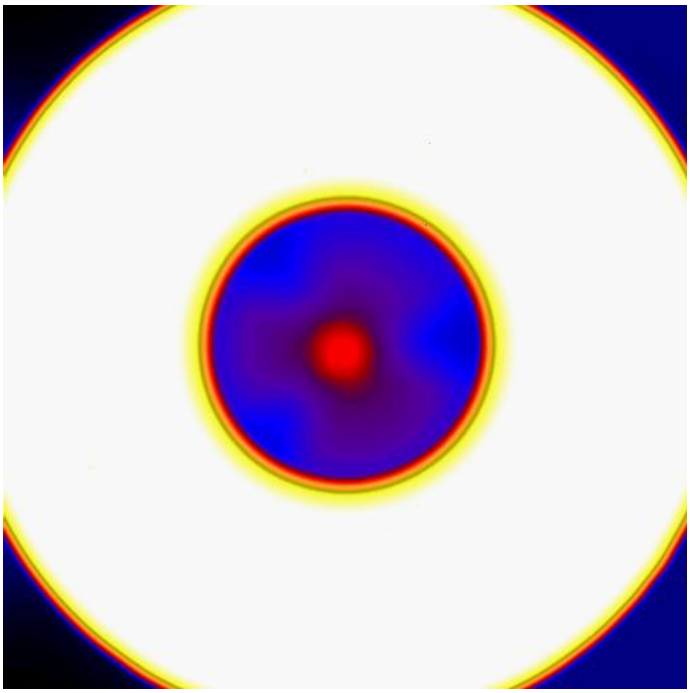

Figure 4. Sample image of COR1-A diffuser window.

Although ostensibly the area inside the occulter should be unilluminated, some signal in that region can be seen in Figure 4, emphasized by the processing of the image. The central red dot is known as the "spot of Arago", and is caused by Fresnel diffraction from the edges of the occulter. The rest of the light inside the occulter is due to scattering within the instrument. This scattered light is asymmetric, and is concentrated in three fan-like directions. This is believed to be due to the three pads holding the objective lens in place. This scattered light component was modeled as having the functional form

$$S(r,\theta) = \exp[A_0(\theta) + A_1(\theta)r]$$

where θ and r represent the polar coordinates of each pixel relative to Sun center, and A_0 and A_1 are parameters fitted at a series of θ values, from 0° to 359° in steps of 1°. This functional form was selected heuristically based on an examination of the data. Figure 5 shows the resulting modelled stray light. The process for deriving the vignetting function is then:

- Subtract the modelled stray light pattern (Figure 5) from the door image (Figure 4)
- Renormalize so that the values in the unvignetted open region are close to unity.
- Select a threshold (0.01) below which the vignetting values are unreliable, and reset these pixels to 1.0 to avoid large overcorrections. Include all pixels within the occulted areas.

Figure 6 shows a trace along the resulting vignetting/flat-field image for COR1-A.

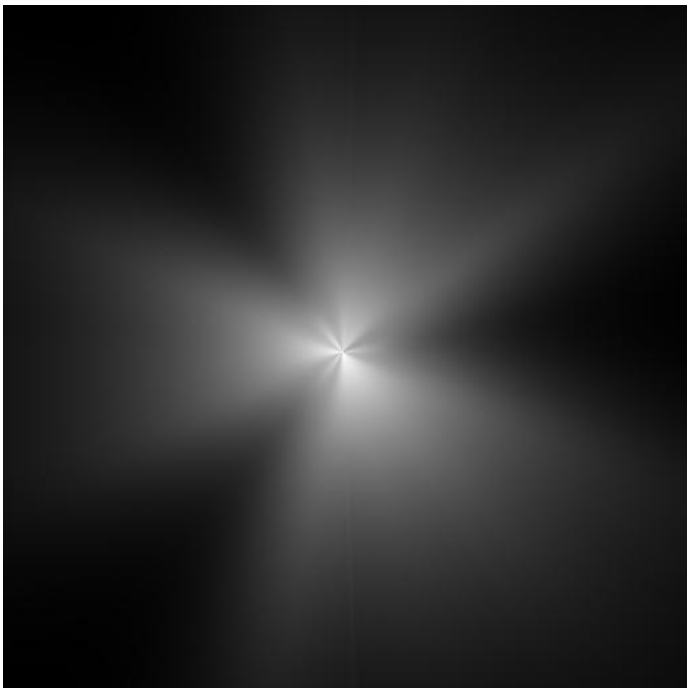

Figure 5. Modeled scattered light for COR1-A door measurements.

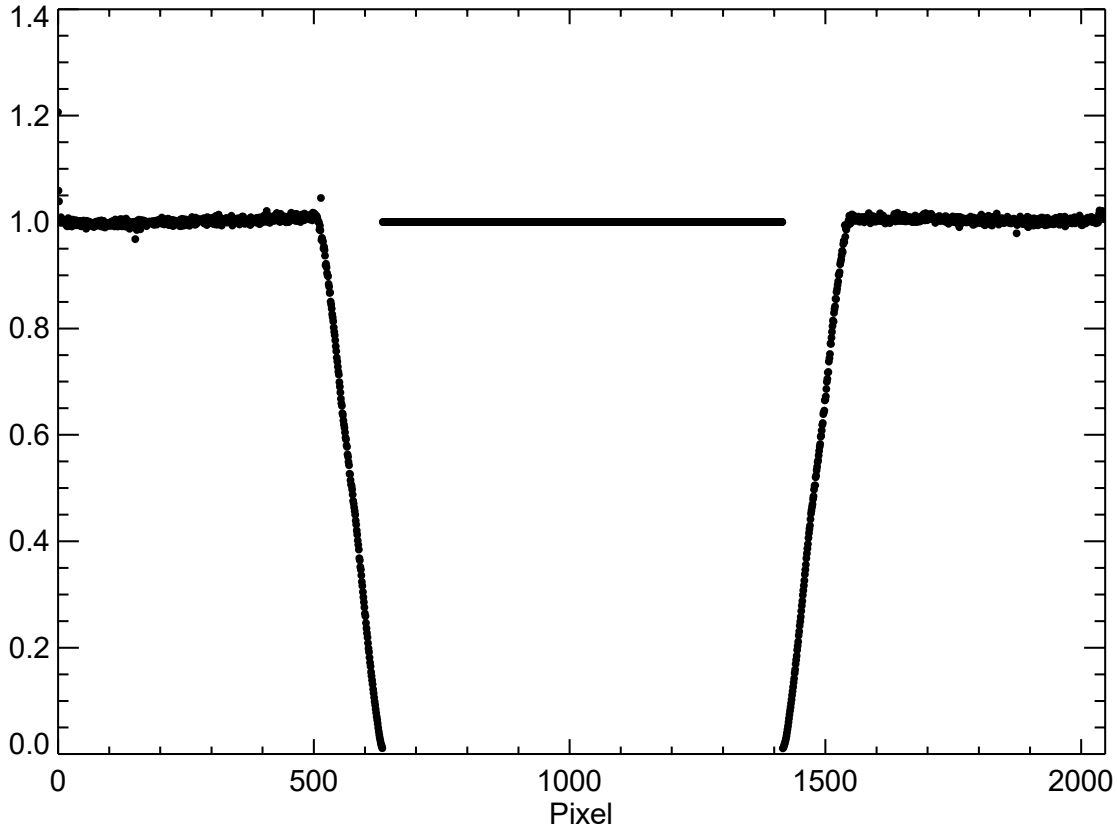

Figure 6. Horizontal trace along center of COR1-A vignetting/flat-field image.

The following table shows the calibration factors derived from the inflight measurements.

Measurement	Quantity	Data Products Affected
Observations of planet Jupiter	Radiometric calibration	Level 1
Occultation of Moon against Sun	COR1-B pointing calibration, plate scale, roll angle	COR1-B Level 0, Level 1
Observations of λ Aquarii	COR1-A pointing calibration, plate scale, roll angle	COR1-A Level 0, Level 1
Door-mounted diffuser	Vignetting function	Level 1
Star monitoring	Monitoring radiometric calibration, pointing	Level 1

2.4.2 Validation

The principal method for validating the COR1 calibration is to compare the data with those from other coronagraphs.

Thompson and Reginald (2008) compared observations of CMEs with simultaneous observations from the SOHO LASCO C2 and the Mauna Loa Solar Observatory (MLSO) Mk4 coronagraphs. Events were chosen from early in the mission when the two STEREO spacecraft were still close to the Sun-Earth line. Total brightness measurements from COR1 were compared against the same from LASCO C2 in the overlapping region from 2.5 to 2.7 $R_\odot$ for two strong CMEs that occurred on the 24th and 30th of January 2007, when the two STEREO spacecraft were only 0.5–0.6 degrees apart. Pre-event images were subtracted from all three telescopes to isolate the CME, and to ensure that the comparison of the radiometric calibrations was unaffected by any errors in the background determination. It was found that the COR1-A and COR1-B results were practically indistinguishable, while the LASCO C2 data were about 20% lower. This test also demonstrated that the three telescopes were well coaligned with each other.

A similar comparison (using polarized brightness) with the MLSO Mk4 coronagraph between 1.5 and 2.8 $R_\odot$ was made by Thompson and Reginald (2008) with a CME that occurred on 9 February 2007, when the two STEREO spacecraft were separated by 0.7 degrees. The Mk4 data were found to be about 50% higher, though this may have been partially due to a sinusoidal pattern in the data which appeared to be elevating the values in the region around the CME. Also, there appeared to be a slight offset in position angle between the Mk4 and COR1 telescopes. Otherwise, good agreement was found between all three telescopes.

Frazin *et al*. (2012) compare observations of the overall coronal structure on 16 April 2007 from the COR1 and COR2 telescopes on both STEREO spacecraft with those from LASCO C2 and MLSO Mk4. They found good agreement within the uncertainties for pB measurements in bright streamer structures from all six telescopes. Difficulty with background subtraction was identified as the biggest problem with inter-telescope comparisons.

Thompson *et al*. (2011) took advantage of the fact that when the two STEREO spacecraft were close to 180° apart on 6 February 2011, they both see the same corona from opposite angles. They found that the relative error between COR1-A and COR1-B was less than 10^{-9} MSB over most of the field-of-view, growing to a few $\times\ 10^{-9}$ MSB for the brighter pixels near the edge of the occulter. Along with the radiometric calibration, these measurements also validated the procedure used to estimate the instrumental background by showing the streamer brightnesses are quite robust.

2.5 References

[SECCHI_PREP] STEREO/SECCHI Level-0.5 to Level-1 Calibration CMAD, STEREO_SECCHI_Prep_CMAD_20211206.pdf, Version 1.1, 06 December 2021

The documents reporting the results of the COR1 pre-flight calibration activities are as follows:

Date	Title
June 2, 2004	COR1-A Final Assembly Tests, May 2004
June 25, 2004	COR1-A Pre- and Post-Vibration Tests, May-June 2004
July 29, 2004	COR1-A Vacuum Calibration, July 2004
September 21, 2004	COR-1B Final Assembly Tests, September 2004
October 2, 2004	COR-1B Pre- and Post-Vibration Tests, September 2004
November 18, 2004	COR-1B Vacuum Calibration, November 2004
December 10, 2004	COR1-A pre- and post-vibe measurements on SCIP bench, November–December 2004
March 24, 2005	COR-1A/B Plate Scale Verification
April 18, 2005	COR1-A Vacuum Recalibration, April 2005
May 19, 2005	COR1-B Vacuum Recalibration, May 2005
June 22, 2005	COR-1B pre- and post-environmental measurements on SCIP bench, February–June 2005

References from the scientific literature concerning in-flight calibration and validation are as follows:

Chanover, N.J., Kuehn, D.M., Banfield, D., Momary, T., Beebe, R.F., Baines, K.H., Nicholson, P.D., Simon, A.A., Murrell, A.S., 1996, Absolute reflectivity spectra of Jupiter: 0.25–3.5 micrometers, *Icarus*, **121**, 351–360.

Frazin, Richard A., Vásquez, Alberto M., Thompson, William T., Hewett, Russell J., Lamy, Philippe, Llebaria, Antoine, Vourlidas, Angelos, Burkepile, Joan, 2012, Intercomparison of the LASCO-C2, SECCHI-COR1, SECCHI-COR2, and Mk4 Coronagraphs, *Solar Phys*., **280**, 273–293.

Thompson, W.T. and Reginald, N.L., 2008, The Radiometric and Pointing Calibration of SECCHI COR1 on STEREO, *Solar Phys.*, **250**, 443–454.

Thompson, W. T., Davila, J. M., St. Cyr, O. C., Reginald, N. L., 2011, STEREO SECCHI COR1-A/B Intercalibration at 180° Separation, *Solar Phys*., **272**, 215–225.

Thompson, W.T., 2018, Sensitivity Monitoring of the SECCHI COR1 Telescopes on STEREO, *Solar Phys.*, **293**, 49 (12 pp).

3. Derivation of Polarization Parameters

3.1 Overview

The polarization properties that can be derived from sets of polarized COR1 images at 0°, 120°, and 240° are:

Quantity	Description
B	Total brightness
pB	Linearly polarized brightness
pB/B	Fractional polarization
μ	Angle of polarization

3.1.1 Heritage

The process of measuring the polarized brightness of the corona has long been known, and is thoroughly described in Billings (1966). The LASCO C2 and C3 coronagraphs on SOHO (Brueckner *et al*., 1995) include the option of rotating a series of linear polarizers into the beam to derive the polarization parameters. The technique used for COR1 is essentially the same, except that instead of rotating multiple polarizers in and out of the beam, a single polarizer remains in the beam at all times and rotates about its optical axis. This greatly simplifies the calibration process by removing the need to cross-calibrate the different polarizers. The MLSO Mk4 coronagraph (Fisher *et al*., 1981) also used linear polarizers to derive pB, but with a different instrument design from that of COR1.

3.1.2 Product Description

The process of deriving the polarization properties from COR1 data takes three images taken in rapid sequence, I_0, I_{120}, I_{240}, and returns three new images, B, pB, and μ, with the same size and format, so that the pixels in the derived images are in a one-to-one relationship with the original images.

3.2 Theoretical Description

By Malus's Law, if the incoming radiation from the corona is composed of both unpolarized I_U and linearly polarized I_P components, then the measured signal I_M after passing through a perfect polarizer will be

$$I_M = \frac{I_U}{2} + I_P cos^2(\mu - \mu_0) \qquad (1)$$

where μ_0 is the angle of the polarizer used to analyze the signal. (Note that $pB = I_P$, and $B = I_U + I_P$.) With an extinction factor greater than 10,000:1, the Polarcor polarizer can be considered to be "perfect" for all practical purposes. The above equation should also include a transmission factor, but this is absorbed into the overall instrumental calibration factor c described in Section 2. From measurements

taken at three different polarization angles μ_0, it is possible to derive the state of polarization. When these three angles are 0°, 120°, and 240°, these relationships simplify to

$$B = \frac{2}{3}(I_0 + I_{120} + I_{240})$$

$$pB = \frac{4}{3}\sqrt{(I_0 + I_{120} + I_{240})^2 - 3(I_0 I_{120} + I_0 I_{240} + I_{120} I_{240})} \quad (2)$$

$$\mu = s\cos^{-1}\sqrt{\frac{I_0 - (B - pB)/2}{pB}}$$

where s represents the sign of μ, and is +1 if $I_{240} > I_{120}$, and -1 otherwise. The above equations are carried out in SolarSoft through the routine `cor1_quickpol.pro`. It's also possible to return polarization parameters directly from SECCHI_PREP. in that case the Stokes parameters I, Q, and U are calculated first, and B, pB, and μ are calculated from the Stokes parameters; however, the results are the same within numerical roundoff limits.

One of the properties of Equation 2 is that pB is always returned as a positive number. An alternative method for calculating pB involves recognizing that Thomson scattered light is always polarized perpendicular to the plane of scattering. This allows one to fix the angle μ for every pixel in the image. In essence, the problem is then reduced to finding the best least-squares fit for the parameters I_U and I_P in Equation 1. The resulting solution for pB reduces to

$$pB = \frac{8}{3}[I_0 cos^2\theta + I_{120} cos^2(\theta - 120°) + I_{240} cos^2(\theta - 240°)] - 2B \quad (3)$$

where θ is the azimuthal angle for each pixel in device coordinates measured around Sun center in the direction of the mechanism rotation. The calculation of B is unchanged. This method for calculating pB in COR1 data, which is implemented in SolarSoft through the routine `cor1_fitpol.pro`, was first discussed in Thompson (2015).

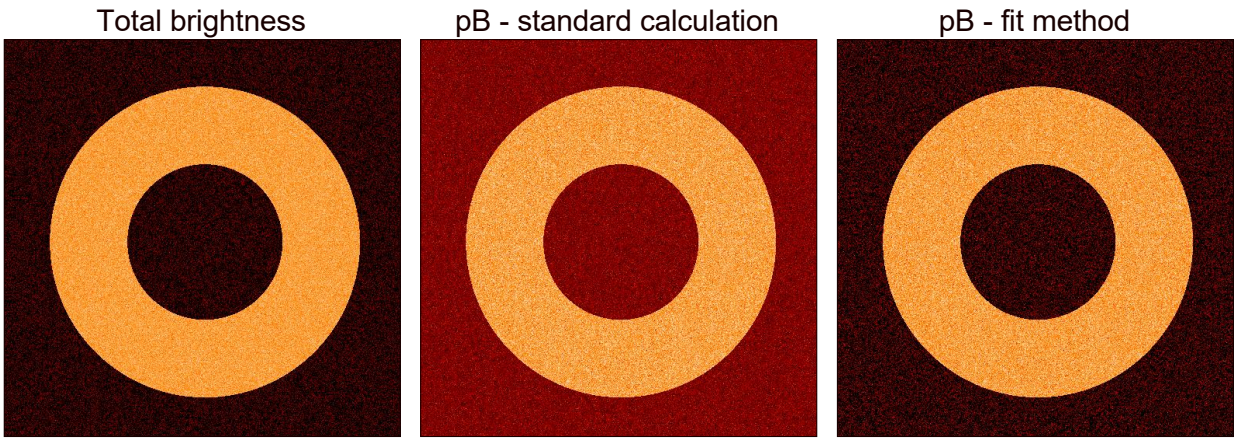

Figure 7. Calculated total and polarized brightness images from simulated data with noise.

The effect of these two different methods of determining pB is demonstrated in Figure 7. A set of three polarization sequence images was generated with a toroidal region of brightness 100 counts and 100% polarization, with the remainder set to zero. Random noise with a standard deviation of 10 counts was then added to these images, which were then processed to calculate the polarization parameters. In Figure 7, the left image is the calculated total brightness, which is the same in both methods, the middle image is pB calculated using Equation 2, and the right image is pB calculated using Equation 3. It is evident that the areas outside of the modelled toroid are darker in the right image than in the middle image, while the brightness of the toroid itself is apparently unchanged. This is shown more quantitatively in Figure 8, where the two techniques are plotted against each other. The data fall into two regimes. One regime, with values near 100, represents the toroidal area—here the two calculations show little difference from each other. The other region, with absolute values below about 50 counts, represents the region outside the toroid, where there should be no signal. Using Equation 2, the average value in this region is $pB = 20.5 \pm 10.7$, while with Equation 3 the average value is essentially zero, with a standard deviation of 16.3. In other words, use of Equation 3 avoids biasing pB values upwards in regions where there is no significant signal.

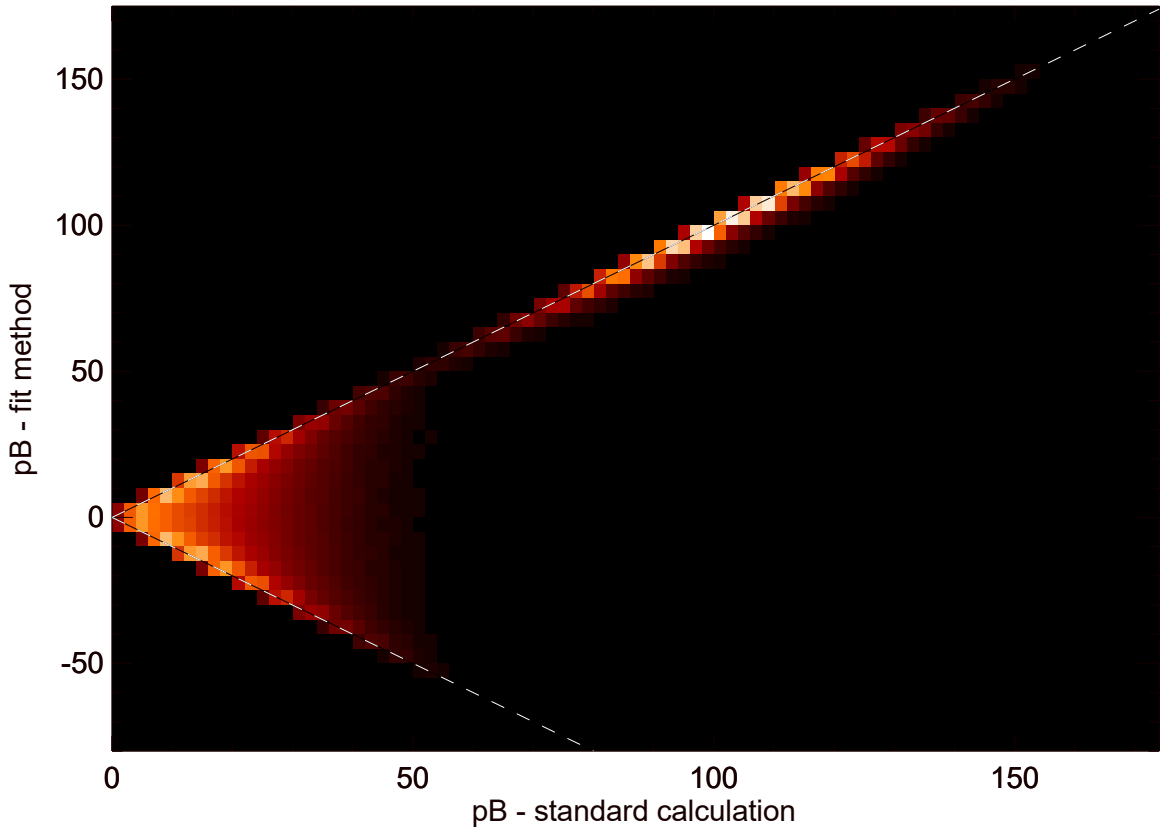

Figure 8. Density plot showing relationship between polarized brightness calculated using the two discussed techniques. The two dashed lines represent where the absolute values in the two techniques would be equal to each other.

Negative pB values returned by Equation 3 actually do have a physical meaning. They represent polarization in the plane of scattering, perpendicular to the polarization direction seen in Thomson

scattering. The distinction between positive and negative polarization is common in the scientific literature discussing scattering from small grains, such as in the tails of comets, and such negative polarization has been studied in sungrazing comets seen by STEREO.

3.3 Error Analysis and Corrections

The statistical uncertainty in the derivation of total brightness is driven by the uncertainty in the individual images making up a polarization sequence (Section 2.3). From Equation 2, one can derive that the uncertainty in total brightness is

$$\sigma(B) = \frac{2}{3}\sqrt{\sigma^2(I_0) + \sigma^2(I_{120}) + \sigma^2(I_{240})}$$

or, since all the images have roughly the same error, $\sigma(B) = \frac{2}{\sqrt{3}}\sigma(I_x) = 1.1547\sigma(I_x)$, where $\sigma(I_x)$ represents the uncertainty of any single image. Roughly speaking, the statistical uncertainty in the derivation of pB is about $\sqrt{2}$ higher than that of B.

Aside from the statistical uncertainty, the *accuracy* of a total or polarized brightness calculation depends on how well the instrumental background can be subtracted. There are several ways background subtraction can be handled. Section 4 discusses the process of estimating the instrumental background based on long-term monitoring of the instrumental signal. For measurements of CMEs, a highly effective technique is to subtract a pre-event image. Not only does this remove the effects of the instrumental background, it also isolates the CME from the relatively unchanging background corona. Note that subtracting a pre-event image increases the statistical uncertainty by $\sqrt{2}$ due to the fact that both images are statistically uncertain. The same is true for running difference images.

3.4 Calibration and Validation

3.4.1 Calibration

Section 2.4.1 completely covers all calibration issues involved in deriving the polarization parameters.

3.4.2 Validation

Validation of the proper functioning of the COR1 polarizers were determined during vacuum testing in the NRL facility. The instrument was exposed to both completely polarized and partially polarized light, and in both cases the correct level and direction of polarization were obtained.

Validation of Equation 3 was obtained by comparison with in-flight results using Equation 2. The results were essentially the same for regions with sufficient signal.

3.5 References

Billings, D. E., 1966, A Guide to the Solar Corona, New York: Academic Press.

Brueckner, G. E., Howard, R. A., Koomen, M. J., Korendyke, C. M., Michels, D. J.; Moses, J. D., Socker, D. G., Dere, K. P., Lamy, P. L., Llebaria, A., Bout, M. V.; Schwenn, R., Simnett, G. M., Bedford, D. K., Eyles, C. J., 1995, The Large Angle Spectroscopic Coronagraph (LASCO), *Solar Phys*., **162**, 357–402.

Fisher, R. R., Lee, R. H., MacQueen, R. M., Poland, A. I., 1981, New Mauna Loa coronagraph systems, *Applied Optics*, **20**, 1094-1101.

Thompson, W. T., 2015, Linear polarization measurements of Comet C/2011 W3 (Lovejoy) from STEREO, *Icarus*, **261**, 122–132.

4. Background determination

4.1 Overview

The most difficult task in analyzing COR1 data is determining the instrumental background. As in all solar coronagraphs, the instrumental background dominates the raw signal from the detector. Figure 9 shows traces through the center of a COR1-A image from January 2008. The black curve shows the raw data, while the red curve shows the inferred K-corona signal, which is typically around two orders of magnitude lower. Note that when we talk about removing the instrumental background, we're also removing scattered light from dust particles in orbit about the Sun, known as the F-corona. The objective of background subtraction is to isolate the K-corona signal due to Thomson scattering.

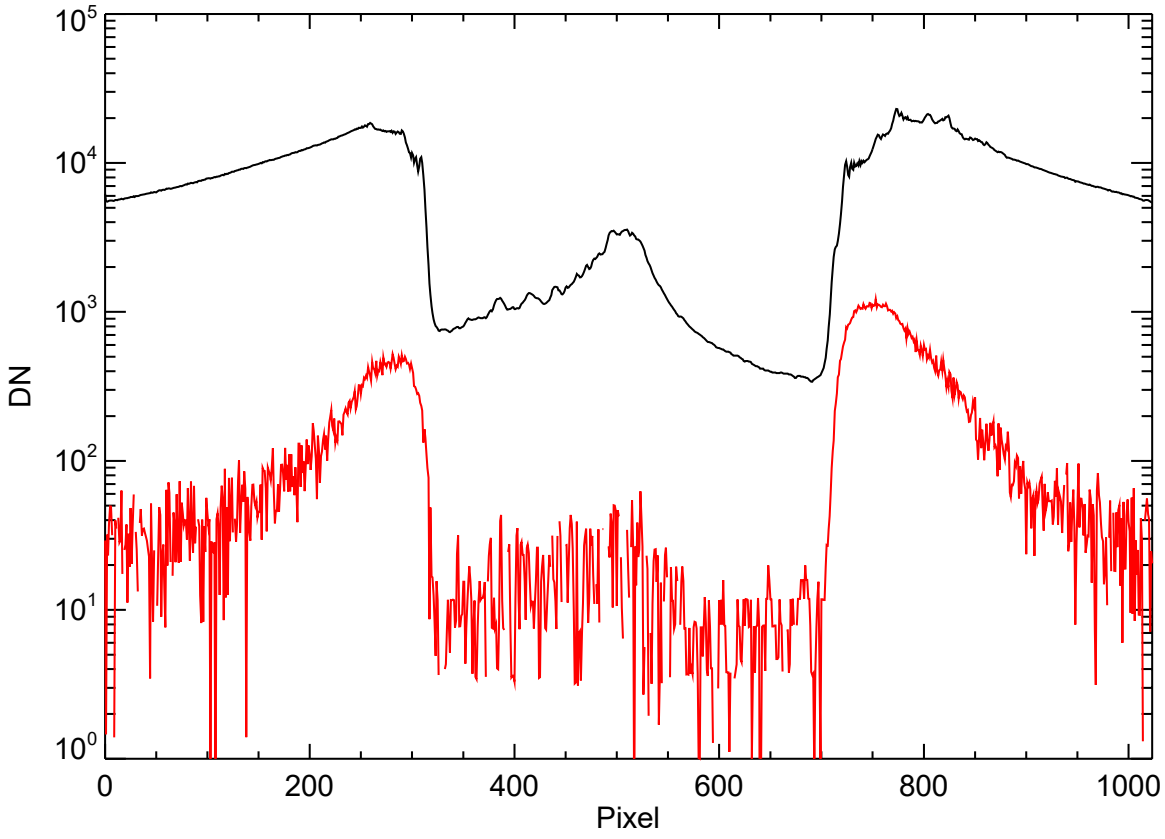

Figure 9. Comparison of raw detector signal (black) with inferred K-corona signal (red) for the COR1-A telescope in January 2008.

The method used for removing the instrumental background depends on the science requirements. For studying transient phenomena such as CMEs, it's most effective to subtract a suitably selected pre-event image, thus isolating the CME from both the instrumental background and the (mostly) quiescent coronal streamers. Running-difference images can also be used effectively to delineate the morphology of CMEs. However, these techniques do not allow one to extract the overall structure of the K-corona. For that, one needs a reasonably accurate estimate of the instrumental (plus F-corona) background. This CMAD describes the method used to estimate such backgrounds, and their subsequent subtraction from the raw data. Figure 9 represents an example of the use of these backgrounds to extract the K-corona signal.

4.1.1 Heritage

The method described in this CMAD is based on procedures used for the SOHO/LASCO telescopes, optimized for COR1.

4.1.2 Product Description

There are four different kinds of background images that can be applied to COR1 data:

Type	Cadence	Description
Daily median	Daily	"Median" image derived from days images
Monthly minimum [default]	Every 10 days	"Minimum" image derived from a month's worth of daily median images
Raw calibration roll	Roughly every three months	Minimum image derived from images taken during a SECCHI stepped calibration roll
Monthly roll	Every 10 days	Combination of monthly minimum and calibration roll data.

Background images are produced at the same resolution as the original images, with each pixel in a one-to-one relation with the raw images. Separate backgrounds are calculated for each polarizer angle, so that the polarization signal within the background is also subtracted out.

A total brightness background is calculated from the average of the three polarized backgrounds. The purpose of the total brightness background is for subtracting from total brightness images that are formed onboard the instrument to reduce telemetry volume. The data for these total brightness images are taken in the same way as the polarization sequence images, except that the three images are averaged onboard into a single image. When needed to reduce telemetry usage, total brightness images are alternated with polarization sequence images. The reason for forming the backgrounds for these images from the polarization sequence backgrounds, instead of directly from the total brightness images, is to ensure that a consistent background is subtracted from all images.

Background images are generated without any calibration factors applied to them, so that they don't need to be regenerated if the calibration factors change. Thus, the backgrounds are not corrected for vignette or flat fielding, and the values are not converted into MSB.

4.2 Theoretical Description

The basic methodology used for estimating the instrumental (plus F-corona) background is to monitor the signal over a full solar rotation, allowing the coronal features to rotate in and out of the field-of-view. The background is then estimated as the baseline signal present in all images. A full description of the process of estimating the background is given in Thompson *et al*. (2010).

The first step in the LASCO method is to generate daily median images formed by stacking all the images into a data cube, and then taking the median value along the time dimension at each pixel position. The purpose of this procedure is to derive a representative image for each day, with most of the noise fluctuations removed, and without transient features such as CMEs. The median is used instead of the minimum to avoid under-correcting due to biasing toward the low end of noise fluctuations. A hybrid approach was adopted for COR1, where each day is split up into multiple blocks. A median image is generated in each block, and then the minimum of all the blocks is calculated. This approach removes additional K-coronal signal resulting from evolution during the day.

Conceptually, monthly minimum images are generated by taking 29 days' worth of daily median images, and calculating the minimum value at each pixel. The actual procedure for COR1 includes corrections for an overall slowly changing brightness over the course of the month, as described in Thompson *et al*. (2010). Monthly minimum images are generated every 10 days, specifically for dates whose Modified Julian Date (MJD) is divisible by 10.

Four times a year each STEREO spacecraft undergoes a maneuver known as the SECCHI Stepped Calibration Roll. Observations are made with the spacecraft rolled to a series of positions at 60° intervals between 0° and 360°, plus stops at 90° and 270°. Backgrounds for each polarizer angle are generated from the minimum of the nine polarization sequences taken during this maneuver. In the SECCHI software, this is known as a "raw calibration roll" background. Such backgrounds are particularly effective when there are well-formed polar coronal holes which can be rolled through all position angles in the image. Stepped calibration rolls are nominally performed near perihelion, aphelion, and at the two points midway between perihelion and aphelion.

The information from the monthly minimum backgrounds and calibration roll backgrounds are combined together into a single product known as the monthly roll backgrounds. When possible, each monthly minimum background has a corresponding monthly roll background. As explained in Thompson *et al*. (2010), the roll backgrounds are first interpolated to the date of the monthly minimum background.

By default, when applied to COR1 data, SECCHI_PREP will automatically subtract the nearest monthly minimum backgrounds, but the other three kinds of backgrounds can be requested instead. The user can also request that linear interpolation be applied between the backgrounds before and after the observation.

4.3 Error Analysis and Corrections

The backgrounds generated by the techniques described in this CMAD can only be considered estimates of the true instrumental background. In particular, any K-coronal signal which is constant over a solar rotation will be absorbed into the background. Therefore, the result of subtracting these backgrounds

will be to isolate those coronal features, such as bright streamers, which are changing over a solar rotation. The incorporation of the calibration roll maneuvers into the background calculations means essentially that the polar coronal holes are used as a reference to which the rest of the corona is compared. Therefore, when using the "monthly roll" backgrounds, one would expect that the measured signal would be lower than the actual K corona at all azimuths by an amount equal to the base signal in the polar coronal holes.

Because the "monthly minimum" and "monthly roll" backgrounds are based on a month's worth of data, it takes time for the backgrounds to settle down to their final state. The backgrounds subtracted from recently downloaded data will tend to be of much poorer quality than what can be done after a few weeks have passed.

To preserve the remaining lifetime of the laser gyros on the STEREO spacecraft, it was decided to turn them off during normal science operations. This "reduced gyro" operations mode began on the *Ahead* spacecraft on 18 September 2013, and on the *Behind* spacecraft on 7 January 2014. Operations without the gyros produced a noticeable "flickering" effect on the COR1 images as the instrumental background shifted back-and-forth across the field-of-view. The result of this on the background determination is that the backgrounds end up being slightly lower in value than they would otherwise be, due to the preferential selection of minimum values at each pixel location.

Changes in the way that the COR1 telescopes are operated—such as changes in pointing, binning, or exposure time—are treated as break points in the background determination and application software. The same is true for sudden changes in the background caused by particles adhering to the objective lens. The dates and times of these changes are kept track of in the SolarSoft routines `cor1_monthly_min.pro` and `scc_getbkgimg.pro`. When forming a background image for a given date, only data on the same side of the break will be considered. Similarly, when subtracting a background, only backgrounds on the same side of the break will be used. For this reason, background subtraction near break points tends to be of lower quality than at other times.

4.4 Calibration and Validation

4.4.1 Calibration

COR1 background images are in instrumental units, with no calibrations applied, to preserve their utility as knowledge of the calibration changes with time.

4.4.2 Validation

Thompson et al. (2010) compared COR1 pB images with simultaneous images from the MLSO Mk4 coronagraph on 2 April 2007, when the separation angle was small. It was found that the background subtraction technique was successful in coronal streamers, while the baseline emission in coronal holes (i.e. between plumes) was suppressed, as expected. Similar results were found in a more comprehensive study of the intercalibration between COR1 and other coronagraphs by Frazin et al. (2012). As discussed in Section 2.4.2, Thompson et al. (2011) compared observations from both COR1-A and COR1-B when the two spacecraft were separated by 180°—and thus seeing the same coronal material from opposite sides—and found excellent agreement in both the radiometric calibration and in the background subtraction.

4.5 References

Frazin, Richard A., Vásquez, Alberto M., Thompson, William T., Hewett, Russell J., Lamy, Philippe, Llebaria, Antoine, Vourlidas, Angelos, Burkepile, Joan, 2012, Intercomparison of the LASCO-C2, SECCHI-COR1, SECCHI-COR2, and Mk4 Coronagraphs, *Solar Phys*., **280**, 273–293.

Thompson, W. T., Wei, K., Burkepile, J. T., Davila, J. M., St. Cyr, O. C., 2010, Background Subtraction for the SECCHI/COR1 Telescope Aboard STEREO, *Solar Phys*., **262**, 213–231.

Thompson, W. T., Davila, J. M., St. Cyr, O. C., Reginald, N. L., 2011, STEREO SECCHI COR1-A/B Intercalibration at 180° Separation, *Solar Phys*., **272**, 215–225.

5. Reconstructions of 3D Electron Density of the Corona

5.1 Overview

Understanding the three-dimensional (3D) electron density distribution in the solar corona is crucial for enhancing observational diagnostics of coronal physical properties, interpreting impulsive events such as coronal mass ejections (CMEs), and validating global magnetohydrodynamic (MHD) models of solar winds (e.g., Jones et al. 2022). The K corona arises from Thomson scattering of photospheric white light by free electrons (*e.g.*, Billings, 1966). Since this emission is optically thin, the observed signal is an integration of contributions from electrons along the entire line of sight (LOS). Deriving electron density in the K corona from total brightness (*B*) or polarized brightness (*pB*) measurements is a classical problem in coronal physics. Due to challenges in separating the K-coronal component from the F-coronal component (see a review by Lamy et al. 2022), which originates from interplanetary dust scattering, *pB* measurements are predominantly used for electron density inversion. This approach is widely accepted because the polarized contribution of the F corona can be neglected within 5 $R_\odot$ (e.g., Hayes et al. 2001).

Rotational tomography provides a robust method for electron density inversion because it does not rely on *a priori* assumptions about the coronal structure. This technique reconstructs the 3D electron density of the global corona using observations from multiple viewpoints, either from different spacecrafts or via solar rotation. Tomographic reconstructions of the 3D electron density have been successfully applied to white-light *pB* images from various instruments, including LASCO/C2, STEREO/COR1, and MLSO Mk4 (see Vásquez 2016 for a review).

5.2 Tomographic Reconstruction

5.2.1 Theoretical Description

It is known that the theoretically predicted polarized K-coronal emission can be expressed as,

$$pB(\rho) = \int_{LOS} K(\boldsymbol{r})\, N_e(\boldsymbol{r})\, d\ell \tag{5.1}$$

where $N_e\ (\boldsymbol{r})$ is the electron density at a position ***r***, and the kernel function $K(\boldsymbol{r})$ models the Thomson scattering (e.g., Billings 1966; Wang et al. 2014).

The principle behind tomographic reconstruction is to recast the inversion of the density integral (Equation 5.1) into a multi-dimensional linear system, $A\boldsymbol{x} = \boldsymbol{y}$, that can be solved numerically. In this context:

- $\boldsymbol{x}$=[x_1,x_2,…, x_n]^T: A column vector containing the unknown densities at all grid points within the computational domain.
- $\mathbf{y}$=[y_1,y_2,…, y_m]^T: A column vector containing the measured data values corresponding to all rays in the utilized images.
- $\boldsymbol{A}$: A matrix with coefficients $a_{i,j}$ (where i=1,..,m and j=1,…,n), which are related to the kernel function $K(\mathbf{r})$.

In practical, instead of solving $A\boldsymbol{x} = \boldsymbol{y}$ directly, the regularized problem is addressed through minimization to stabilize the solution and reduce artifacts caused by data noise and gaps (e.g., Frazin & Janzen 2002; Kramar et al. 2009; Wang et al. 2025),

$$\min_{\boldsymbol{x}} F = \|A\boldsymbol{x} - \boldsymbol{y}\|^2 + \mu \, \|R\boldsymbol{x}\|^2 \qquad (5.2)$$

where the matrix R represents a finite difference approximation, and μ is the regularization parameter, controlling the trade-off between the fidelity to the data and the regularization term. Increasing μ leads to a smoother solution, while decreasing μ allows the solution to fit the data more closely. The optimal value of μ can be determined by cross validation (CV). The minimization problem described in Equation (5.2) can be efficiently solved using the standard conjugate gradient (CG) method, which iteratively minimizes the quadratic function.

5.2.2 Applications for COR1 *pB* Observations

Kramar et al. (2009) first applied the tomography technique to STEREO/COR1 *pB* images, to reconstruct the 3D electron density of the corona. They found that the rapid decrease of *pB* signals with height could result in linear artifacts in the reconstruction. To mitigate this effect, they proposed applying a weighting factor, $w = 1/I_{\mathrm{bg}}(r)$, in the first term of Equation (5.2), where $I_{\mathrm{bg}}(r)$ represents the background *pB* at a given radial distance *r*. Wang et al. (2025) further refined this approach by incorporating radial weighting into the regularization term. Their study demonstrated that radial weighting helps achieve balanced smoothing across different heights, allowing for the recovery of finer structures at lower heights while stabilizing the solution and preventing oscillatory artifacts at higher altitudes.

Tomographic reconstructions typically rely on data collected over approximately half of a solar rotation by a single spacecraft. However, a shorter data-gathering window can be achieved when observations from multiple vantage points are available. For example, a reconstruction using data from a single spacecraft (e.g., COR1-B) requires approximately 27–28 *pB* images sampled at 12-hour intervals. Images affected by CME activity or significant instrumental noise are replaced with clean, relatively stable images taken within ±12 hours, if available (otherwise, excluded). After despike processing, the images are rebinned to a 128×128 format, and the radial background intensity, $I_{\mathrm{bg}}(r)$, is computed as the global average of all these images.

The 3D electron density can be determined using either Cartesian or spherical grids (see Fig.10). In the Cartesian grid case, a 128^3 grid in Carrington coordinates is used with a spherical domain defined by $R_{\mathrm{in}} - 2ds \leq r \leq R_{\mathrm{out}} + 2ds$, where R_{in} =1.5 $R_\odot$ and R_{out} =4.0 $R_\odot$ represent the inner and outer boundaries of

data points in each image. The grid size is set to *ds*=0.063 $R_\odot$. The solution domain is chosen slightly larger than the data range to reduce boundary effects.

For the spherical grid, a 361× 181× 51 voxel structure is used in the longitudinal, latitudinal, and radial directions, respectively. This configuration results in a bin size of 1° in longitude and latitude and a radial bin size of 0.05 $R_\odot$. The inversion is conducted within the domain of $R_{in} \leq r \leq R_{out}$, with data sampling consistent with the Cartesian grid case.

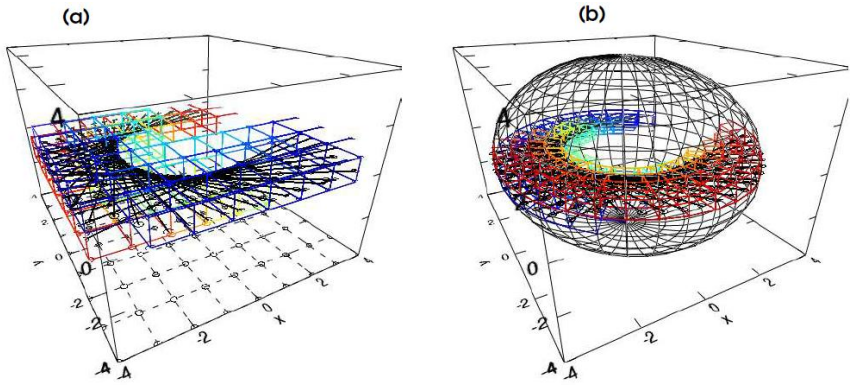

Figure10. Illustration of the tomographic reconstruction of coronal density in (a) Cartesian grid and (b) spherical grid. The 28 rays, corresponding to a given data point in 28 successively observed images over two weeks by COR1-B, are shown as black lines, while the intersected cells are indicated by colored lines.

5.3 Error Analysis and Validation

For reconstructions using a spherical grid, tests with a reduced grid resolution (181×91×51) or a higher image sampling cadence of 6 hours yield similar results. This suggests that the primary factor influencing the spatial resolution of the reconstructed density is neither the grid resolution nor the image sampling cadence, but rather the validity of the assumption that the coronal density remains static during the data collection period. As a result, the reconstructed solutions should represent density structures that are either stable or evolving slowly enough to persist over the given period. A detailed evaluation of single-spacecraft tomographic reconstructions is provided in Wang et al. (2025), where comparisons with MHD simulations and multi-viewpoint tomography reconstructions are discussed.

Some negative-density artifacts appear in the solutions obtained with the employed method. This may stem from the ill-posed nature of tomography, where small variations in data or noise can lead to instability in the solution, occasionally producing unphysical negative values (see, e.g., Kramar et al. 2009). Note that negative values in final density reconstructions are set to be zero.

5.4 Description of 3D Electron Density Product

A tomography inversion code in FORTRAN-90 for both Cartesian and spherical grids has been developed and is publicly available via Github. Tests based on STEREO/COR1 data show that the results produced by the two grids are in good agreement. Using this code with $I_{\mathrm{bg}}(r)$ weighting in regularization, reconstructions of the 3D density for CRs 2052 to 2154 (two per CR) were calculated using

STEREO/COR1B data, covering the period from 2007-01-08 to 2014-09-17, with a spherical grid of 361 × 181 × 51 in longitude, latitude, and radial direction. The dataset of these reconstructions, in the standard FITS format can be accessed on the SSC website.

5.5 References

Billings, D. E., 1966, A Guide to the Solar Corona, New York: Academic Press.

Frazin, R.A., Janzen, P.: 2002, Tomography of the Solar Corona. II. Robust, Regularized, Positive Estimation of the Three-dimensional Electron Density Distribution from LASCOC2 Polarized White-Light Images. Astrophys. J. 570, 408.

Jones, S.I., Wang, T.J., Arge, C.N., Henney, C.J., Uritsky, V.M., Rura, C.: 2022, Quantitative Evaluation of Coronal Magnetic Field Models Using Tomographic Reconstructions of Electron Density. Astrophys. J. 928, 131.

Kramar, M., Jones, S., Davila, J., Inhester, B., Mierla, M., 2009, On the Tomographic Reconstruction of the 3D Electron Density for the Solar Corona from STEREO COR1 Data. Sol. Phys. 259, 109.

Lamy, P. L., Gilardy, H., & Llebaria, A., 2022, Observations of the Solar F-Corona from Space, Space Sci. Rev., 218, 53.

Vásquez, A.M., 2016, Seeing the solar corona in three dimensions. Advances in Space Research, 57, 1286.

Wang, T.J., Davila, J.M., 2014, Validation of Spherically Symmetric Inversion by Use of a Tomographically Reconstructed Three-Dimensional Electron Density of the Solar Corona. Sol. Phys. 289, 3723.

Wang, T.J., Arge, C.N., and Jones, S.I., 2025, Improved Tomographic Reconstruction of 3D Global Coronal Density from STEREO/COR1 Observations, Sol. Phys., Accepted.